3-D modelling of Alpine Mohos in Southwestern Alps

D. Schreiber, J.-M. Lardeaux, Guillaume Martelet, Gabriel Courrioux, Antonio Guillen

Geophysical Journal International

Geophys. J. Int. (2010) **180,** 961–975 doi: 10.1111/j.1365-246X.2009.04486.x

3-D modelling of Alpine Mohos in Southwestern Alps

Dimitri Schreiber,[1] Jean-Marc Lardeaux,[1] Guillaume Martelet,[2] Gabriel Courrioux[2] and Antonio Guillen[2]

[1] *Université Nice Sophia-Antipolis, UMR Géosciences Azur, Parc Valrose,* 06108 *Nice cedex* 02*, France. E-mail: dimitri.schreiber@unice.fr*
[2] *BRGM,* 3*, Avenue Claude Guillemin,* 45060 *Orléans cedex* 02*, France*

Accepted 2009 December 15. Received 2009 November 27; in original form 2008 July 10

SUMMARY

We present and discuss a 3-D geometrical model of the Moho topography in the Southwestern Alps. To achieve this objective, we used the potential of 3-D modelling software (i.e. a 3-D GeoModeller) to combine gravity, seismic and seismological constraints in a same and coherent 3-D space.

A new regional Bouguer gravity anomaly map of the Southwestern Alps was calculated and filtered to isolate the Moho signature in the Southwestern Alps. Then, two alternative 3-D models were computed with data from the literature based on seismic and seismological constraints. The first one represents an European lithospheric mantle decoupled from the European orogenic crust which is back-thrusted by the Ivrea body whereas the second 3-D model illustrates the subduction of a 20-km-thick piece of lower continental crust, coupled with the European upper mantle, beneath the Ivrea body. According to the geological knowledge of these units we then assigned a density value to each modelled layer and we computed their gravity effects to compare them with the filtered Moho map of the Southwestern Alps. First of all, the significant discrepancies of the Moho gravity signature generated by these two geometrical models reveal that subduction of continental crust is no more active in the present-day configuration of the Southwestern Alps. Therefore, the first 3-D model was refined by a stochastic 3-D gravity inversion.

Based on this processing, our investigations confirm the presence of three superposed Mohos in the Southwestern Alps and underline that:

(i) The crust/mantle European boundary is localized around 50 km depth beneath the Argentera-Mercantour massif,
(ii) The European lithospheric mantle is decoupled from the European orogenic crust,
(iii) The Adriatic mantle (Ivrea body) is split into two distinct units; the upper unit is located at 10 km depth beneath the Dora-Maïra massif, and the lower unit extends from 20 to 45 km depth.
(iv) These two mantle indenters affect differently the European crust and are responsible for the localization of crustal deformation and for strain partitioning in the Southwestern Alps.

Key words: Probability distributions; Gravity anomalies and Earth structure; Mantle processes; Seismicity and tectonics; Dynamics of lithosphere and mantle; Crustal structure.

1 INTRODUCTION

In the Alps, the lithosphere as well as the Moho topography were imaged by geophysical experiments since the fifties (see discussions in Schmid & Kissling 2000 with references therein). According to these investigations, the crustal scale geometry shows that the European Moho deeps progressively eastward and underthrusts the south dipping Adriatic Moho which remains subhorizontal at shallower depth (Roure *et al.* 1996; Waldhauser *et al.* 1998). This shallow depth piece of Adriatic mantle imaged for the first time in the 1960s is classically described as the Ivrea body or anomaly (Closs & Labrouste 1963; Ménard & Thouvenot 1984). The precise geometry of this Moho topography was well documented in the northern part of the western Alps and particularly along the ECORS-CROP profile (Roure *et al.* 1990, 1996; Pfiffner *et al.* 1997). Recently, reliable geophysical data, including local earthquake tomography, gravity modelling and explosion-seismology experiments, were released in the Southwestern Alps, improving the European Moho image and the Ivrea body shape (Masson *et al.* 1999; Paul *et al.* 2001; Vernant *et al.* 2002; Béthoux *et al.* 2007; Thouvenot *et al.* 2007). In spite of these recent geophysical investigations, the crustal scale 3-D geometry of Alpine Mohos topography in the

Southwestern Alps is still a matter of debate (Paul *et al.* 2001; Béthoux *et al.* 2007). Improving the knowledge of this 3-D complexity is crucial for understanding lithosphere dynamics and earthquake location in the Southwestern Alps.

In the last decades, significant progress has been achieved in 3-D numerical modelling of complex geological structures by the development of 3-D modelling software (i.e. 3-D GeoModeller) capable at once of elaborating a 3-D geometrical model from geophysical and geological constraints and of refining it by inversion processes (Martelet *et al.* 2004; Calcagno *et al.* 2008; Guillen *et al.* 2008). Therefore, according to this 3-D modelling technique, we propose in this paper to combine all the available geophysical data in Southwestern Alps in order to constrain the Moho topography and to integrate geologic cross sections and earthquakes locations in a 3-D crustal scale model.

To gain a better knowledge of the Moho topography.

(1) We prepared a new Bouguer gravity map of the Southwestern Alps and filtered it to isolate the Moho signature.

(2) We compiled a Moho model based on seismic reflection and refraction data as well as seismologic data (i.e. local earthquake tomography) available in the literature.

(3) Using 3-D GeoModeller, we computed the gravity fit for the crust–mantle geometries from this model.

(4) We inverted gravity data to further improve the gravity fit starting from the 3-D model.

Finally, we discuss the tectonic evolution and the earthquake distribution of the Southwestern Alps in light of our 3-D refined model.

2 GEOLOGICAL CONTEXT

The Alpine belt, located along the plate boundary between Eurasia and Adria (Apulia), results from the subduction of a Jurassic–Cretaceous ocean followed by the continental collision between two continental margins (see review in Coward & Dietrich (1989)). We focus on the Southern part of the Western Alpine Arc: Fig. 1 represents the simplified tectonic map of the study area. In this area, the west-verging structure derives from the European margin and an oceanic accretionary wedge deformed during the Tertiary. A major thrust zone, the 'Penninic Frontal Thrust' (PFT), separates an External Arc from an Internal Arc whereas eastward, the Internal Arc is bounded by a subvertical strike-slip system corresponding to the Insubric Line (Fig. 1) and separating the Internal Alpine Arc from the Adriatic continental margin (Southern Alps).

The deep structures of the western Alps were defined at the end of the 1970s by compiling all the seismic profiles available at that time (Sapin & Hirn 1974; Thouvenot & Perrier 1980). After Ménard (1979), Fig. 2(a) the Ivrea body represents a mantle flake disconnected from the autochthonous European Moho. Grellet *et al.* (1993) (Fig. 2b), characterized the area between the Pelvoux massif and the Mediterranean coast as a banana-shaped, 47-km-deep crustal root. Later, using 2-D derived controlled-source seismic reflector data, Waldhauser *et al.* (1998) obtained structural information of the crust–mantle boundary (see Fig. 2c). This led them to a revised 3-D topography of the Moho and lateral continuity of seismic interfaces. Due to the lack of seismic data coverage in the SouthWestern Alps, the Waldhauser *et al.* (1998) Moho model results rather from an extrapolation than an interpolation of the seismic data. However, they proposed to distinguish an European, an Adriatic and a Ligurian Moho, with the European Moho subducting below the Adriatic Moho (Ivrea body in our study area) and with the Adriatic Moho underthrusting the Ligurian Moho. In 2000, broadband receiver functions analysis were also used to evaluate the fine-scale *P*-velocity structure of the lithosphere (Bertrand & Deschamps 2000) from 30 selected teleseismic events recorded at three seismological stations of the French TGRS network in the southernmost part of the French Alps. This method provided a punctual Moho depth value below the STET, CALF and SAOF stations respectively, 30, 20 and 23 km (see Fig. 2a). These values are compatible with the Moho maps of Ménard (1979) and Grellet *et al.* (1993) excepted at the CALF station where the Moho depth value is shallower than proposed by Ménard (1979) and Grellet *et al.* (1993).

The last investigation (explosion seismology experiment) was carried out in the framework of GeoFrance 3-D program (1998–2003) in an area between the Pelvoux, Dora-Maira and Argentera-Mercantour massifs (Thouvenot *et al.* 2007; Fig. 2d). This produced the most reliable information on the European Moho depth in the Southwestern Alps. Moreover, local earthquakes tomography studies have significantly improved our knowledge of the crustal structure of the belt and particularly the shape of the Ivrea body (Paul *et al.* 2001; Béthoux *et al.* 2007). These recent seismic and seismologic data were selected to restore the 3-D geometry of the Moho topography in the Southwestern Alps.

3 GEOPHYSICAL DATA ON THE SOUTHWESTERN ALPS

3.1 Gravity data

3.1.1 Regional Bouguer gravity anomaly map

For the computation of our Bouguer gravity map, we mainly used ground gravity data from the French gravity database (Grandjean *et al.* 1998; Martelet *et al.* 2002) and particularly from the gravity surveys performed in the western Alps (Masson *et al.* 1999). Italian gravity data are provided by the BGI (Bureau Gravimétrique International). Both data sets are tied to the international IGSN71 gravity reference and reduced to complete Bouguer anomalies (including terrain corrections within a radius of 167 km), with a reduction density of 2670 kg m^{-3}. The topography used in the computation process of our Bouguer gravity map is provided by a 1000-m resolution DEM. This DEM was derived from the Shuttle Radar Topography Mission (SRTM, NASA) for the French part and from a DTM provided by the Centro di Sudi sulla Geodinamica delle Catene Collisionali (CNR, Italy; Bigi *et al.* 1990) for the Italian zone. Taking into account the original repartition of the gravity data (Fig. 3) and the scale of the geological objects, which are addressed in this study, we build a 2 × 2 km grid using standard minimum curvature algorithm.

The resulting regional Bouguer gravity map presented as Fig. 3 reflects the complexity of the Moho topography in the studied zone. In first order, we recognized a large positive anomaly zone in the eastern and southern part of the studied area whereas the northwestern part represents a vast negative anomaly domain. In the details, we observe behind the trace of the PFT a positive gravity anomaly zone corresponding to the so-called Ivrea body. This latter interpreted as a mantle slice wedged into the European crust (Schmid & Kissling 2000) is precisely located beneath the Dora Maïra massif (Figs 1 and 3). The Eastern part of the studied area is also characterized by a positive anomaly domain, which goes on southward to the Ligurian basin. On the other hand, the northwestern part of

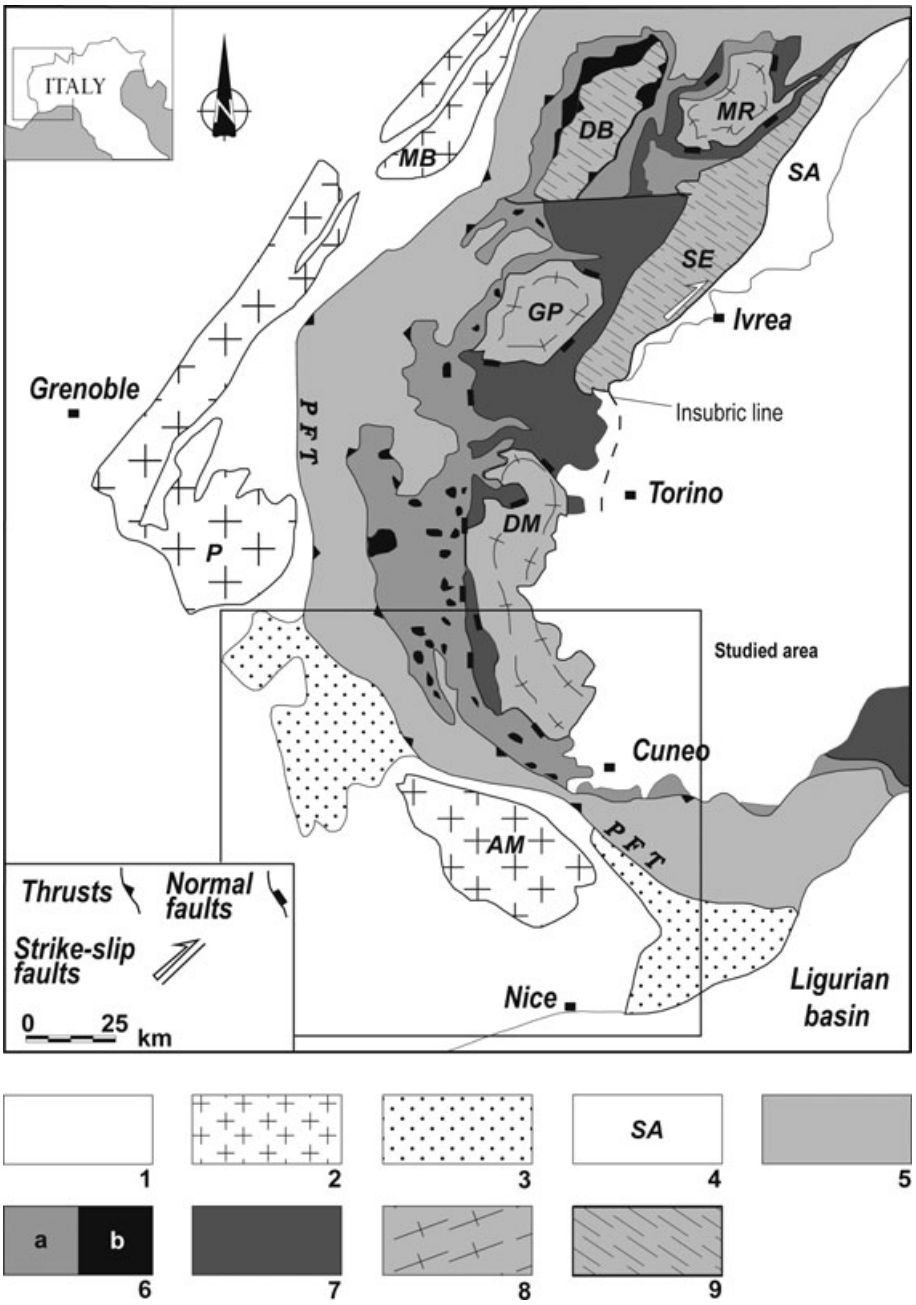

Figure 1. Simplified tectonic map of the western Alps. Alpine External arc and Apulian interland with: (1) Helvetic-Dauphinois domain and Po plain sediment; (2) external crystalline massif (AM, Argentera-Mercantour; P, Pelvoux; MB, Mont Blanc); (3) Heminthoid flysch nappes; (4) SouthAlpine zone, Alpine internal arc with: (5) Briançonnais zone; (6) Blueschist facies Piedmont zone [(a) Schistes lustrés; (b) ophiolites]; (7) eclogite facies Piedmont zone; (8) internal crystalline massif (DM, Dora-Maira; GP, Gran Paradiso; MR, Monte Rosa); (9) Austroalpine units (SE, Sesia; DB, Dent Blanche); PFT, Penninic Frontal Thrust, modified from Lardeaux *et al.* (2006).

our Bouguer anomaly map shows a negative gravity anomaly zone. From the northwest to the south, the gravity anomaly progressively increases from −164 mGal to reach the maximum value of 41 mGal in the Ligurian Basin.

3.1.2 Regional Bouguer gravity map of the Moho signature

In the following sections we focus on the modelling of the Moho interface. To use the gravity data as a constraint for modelling the Moho interface, we removed the short wavelengths of the gravity anomaly. These wavelengths are caused by shallow depth density heterogeneities. Trying to fit these short wavelength anomalies while modelling deep crustal density heterogeneities (the Ivrea body and Moho undulations) would introduce erroneous geometries of the deep crustal effects, which we are interested in.

To achieve a frequency separation as realistic as possible, we first computed the gravity effect of the European Moho geometry proposed by available seismic investigations and studied its frequency content. In Fig. 4, the radially averaged power spectrum of the gravity effect of the seismic Moho exhibits a straight portion of slope α (in the greyed zone) which corresponds roughly to the average Moho depth [computed as 1/2 of the slope of the spectrum

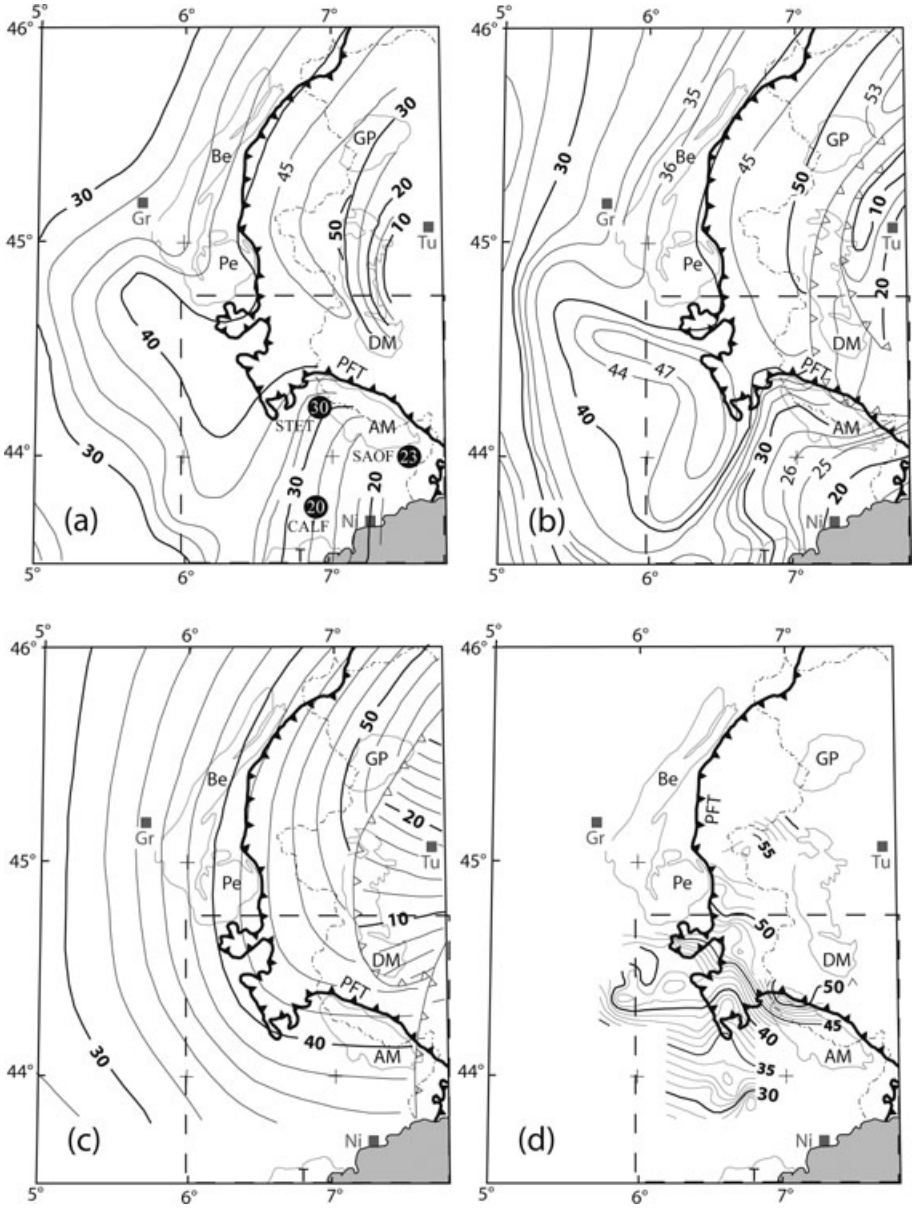

Figure 2. Comparison between four Moho maps in the Southwestern Alps modified after Thouvenot *et al.* (2007): (a) from Ménard (1979) with Bertrand & Deschamps (2000) punctual Moho depth, (b) from Grellet *et al.* (1993), (c) from Waldhauser *et al.* (1998) and (d) from Thouvenot *et al.* (2007). On each Moho map, the curves represent the Moho depth values. The mantle thrusts are symbolised by thin lines and white triangle. Cities: Gr, Grenoble; Ni, Nice; Tu, Turin. Geological units: Be, Belledonne; Pe, Pelvoux; AM, Argentera-Mercantour; DM, Dora-Maira massif; GP, Gran Paradiso; PFT, Penninic Frontal Thrust; T, Tanneron. Studied area is represented by dashed lines. Projection latitude/longitude coordinates are according the WGS84 grid.

(Spector & Grant 1970)]. Therefore, this part of the spectrum reflects the characteristic spectral signature of the Moho. To derive the amount of filtering that is necessary to apply to the Bouguer anomaly to recover a comparable spectral signature, we low-pass filtered the Bouguer anomaly with cut-off wavelengths of 30, 65 and 100 km and computed their power spectrum (Fig. 4). Edge effects in low-pass filtering have been avoided performing the standard windowing, tapering and regional trend removing prior to the Fourier transform.

Spectra derived from progressive filtering of surface Bouguer anomalies show that in the range of wavelengths greyed in Fig. 4, a frequency content roughly equivalent to the one of the Moho effect can be achieved when filtering the gravity anomalies around 65 km. Indeed, the slope and lower inflection point of the spectra of the Moho gravity effect and 65-km-low-pass filtered Bouguer anomaly map are comparable. We therefore applied such filtering to the original Bouguer anomaly map and obtain the long wavelengths gravity anomaly map of the Southwestern Alps presented in Fig. 5. Compared to the original Bouguer map, this filtered gravity map does not contain local variations, whereas the average too long wavelengths of the original map are preserved; that is effects of intermediate to deep crustal density heterogeneities. Even if the top of the Ivrea body is relatively shallow, around 10 km depth, its horizontal extension is large enough to generate a middle-wavelength gravity anomaly which is preserved by the low-pass filtering of the Bouguer anomaly (compare NE part of Figs 3 and 5).

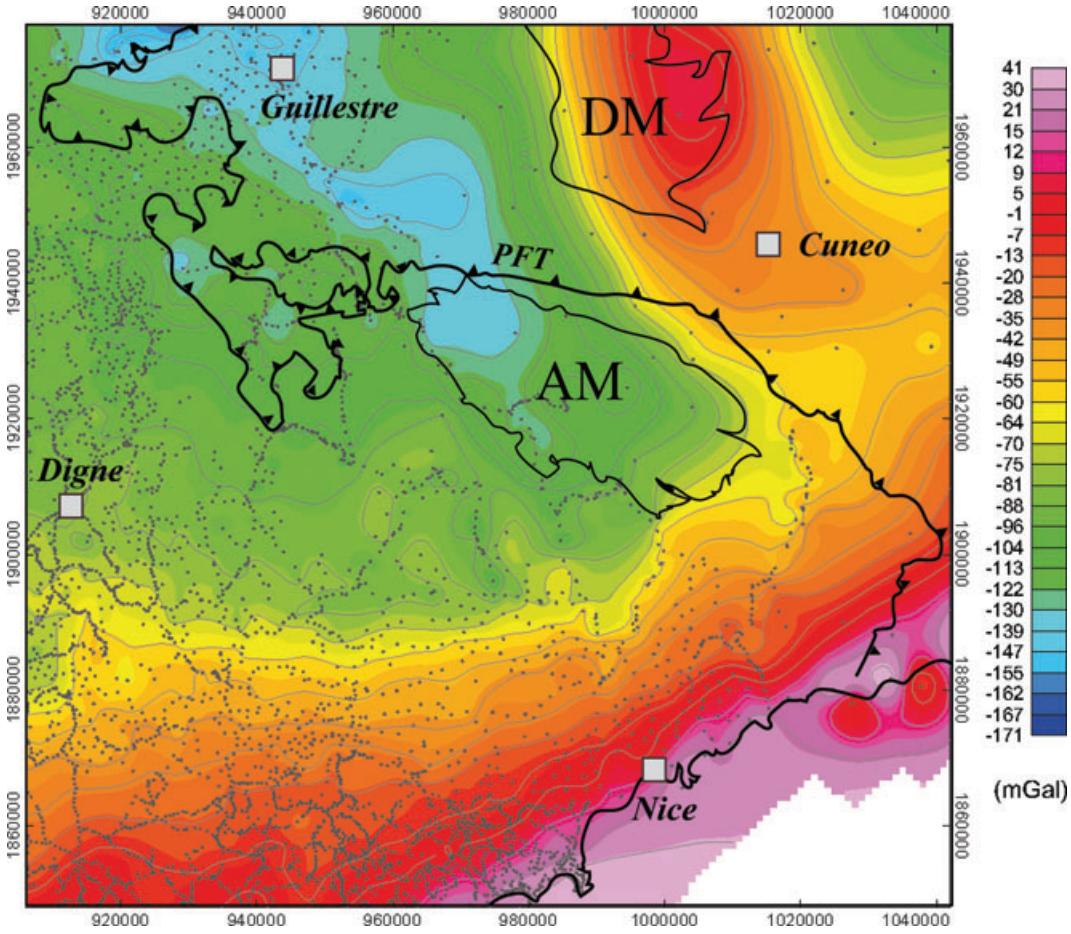

Figure 3. Regional Bouguer gravity map of the studied zone computed by interpolation of gravity data. Geological units: AM, Argentera-Mercantour massif; DM, Dora-Maïra massif; PFT, Penninic Frontal Thrust. Grey dots represent the location of gravity data collection. Projection latitude/longitude coordinates are according the Lambert II extended system.

3.2 Seismic and seismological data

The deep seismic structures of the Southwestern Alps were established by Thouvenot *et al.* (2007). This latter study represents the only direct and thus reliable measurements of the European Moho depth (Fig. 2d). Crustal thickening is imaged from Nice hinterland (Moho depth of 27 km) to the orogenic root zone (Moho depth at 55 km). The zone just south of the Pelvoux massif is characterized by a rather flat, 40-km-deep Moho, which distorts the isobaths in thickening the crust along the Durance valley. Beneath the Argentera massif and just north of it, the Moho map evidences a strong deepening of the Moho down to 51 km (Fig. 2d). The resulting Moho map, drawn integrating depth data measured at ∼300 reflection midpoints, shows a better definition of the European Moho topography than those previously published.

In the Southwestern Alps, local earthquakes tomography studies significantly improved our knowledge of the crustal structure of the belt and particularly the shape of the Ivrea body (Paul *et al.* 2001; Béthoux *et al.* 2007). In these works, The Ivrea body appears as a 10–30 km thick north–south elongated high-velocity anomaly beneath the Dora Maïra massif and extending to the south beneath the northern border of the Argentera-Mercantour massif with a slight eastward plunge.

Both seismic and seismologic data set constitute the geometrical constraints of the 3-D modelling process. The applied methodology used in data integration and the 3-D modelling process are described in the following section.

4 3-D MODEL OF ALPINE MOHOS

4.1 3-D geological modelling principles

Our 3-D analyses were performed using the '3-D GeoModeller' software developed conjointly by the French Geological Survey (BRGM) and Intrepid Geophysics Company. This software was developed specifically for geological applications in order to combine geological and geophysical data available in a single 3-D space. It has recently been used successfully to produce 3-D geological models of complex tectonic structures (Martelet *et al.* 2004; Calcagno *et al.* 2008).

4.2 3-D building process

To build our 3-D model, we used the Moho map proposed by Thouvenot *et al.* (2007) (Fig. 2d) and the local earthquake tomography computed by Paul *et al.* (2001). First of all, we started the modelling process with geo-referencing the Moho map (Fig. 2d) in the 3-D GeoModeller. The isobaths curves traces [from 28 km deep to 51 km deep in the studied zone (Fig. 2d)] were digitalized in

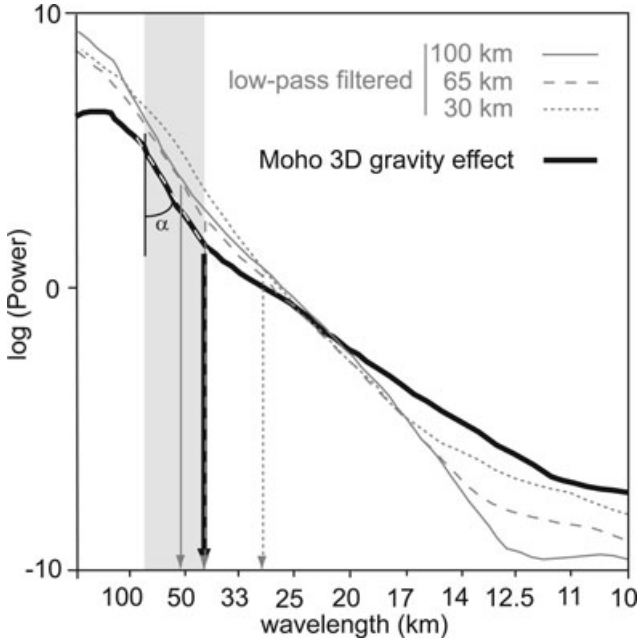

Figure 4. Comparison of spectra derived from progressive filtering of surface Bouguer anomalies. The grey portion of the spectrum corresponds to sources at the Moho depth following the work by Spector & Grant (1970). The bold line represents the gravity effect of a realistic Moho geometry and α the slope of the spectrum. The 65-km-low-pass filtered Bouguer anomaly spectrum is comparable to the spectrum of the Moho gravity effect in term of slope and lower inflection point.

horizontal cross-sections generated at the depth corresponding to the Moho depth defined by each curve. Therefore, this preliminary 3-D model represents the topography of the European Moho. However, the Thouvenot *et al.* (2007) Moho map being incomplete in the eastern part of the area of interest and particularly in the Ligurian Moho realm, we implemented our previous 3-D model with the Waldhauser *et al.* (1998) Moho depth values.

Regarding the integration of the local earthquake tomography constraints and the 3-D modelling of the Ivrea body shape, we imported in the 3-D GeoModeller a 3-D seismological tomography grid (*Vp* values) provided by Paul *et al.* (2001) with a maximal resolution until 30 km depth. The Ivrea body being characterized by a strong *Vp* velocity gradient corresponding to the *Vp* isovalue equal to 7.0 km s^{-1}, we therefore calculated the 3-D geometry of the Ivrea body using this *Vp* isovalue.

Finally, the 3-D geometrical model combining the available geophysical data from Waldhauser *et al.* (1998), Paul *et al.* (2001) and Thouvenot *et al.* (2007), is presented in Fig. 6. The latter is the first 3-D representation of the superposed Mohos in the Southwestern Alps composed by three modelled layers: The Ivrea body, the upper mantle and the orogenic crust.

In this model, the Ivrea body appears split into two distinct units. The first one is localized beneath the Dora Maïra massif at around 10 km depth and stops abruptly at around 17 km depth. The second unit expands between around 20–21 km and 30 km depth. The Ivrea body remains separated in two pieces even if we calculate the model with *Vp* values of 6.9 and 6.8 km s^{-1}.

Taking into account the complex collisional setting of the Southwestern Alps, an alternative, more complex, model involving a

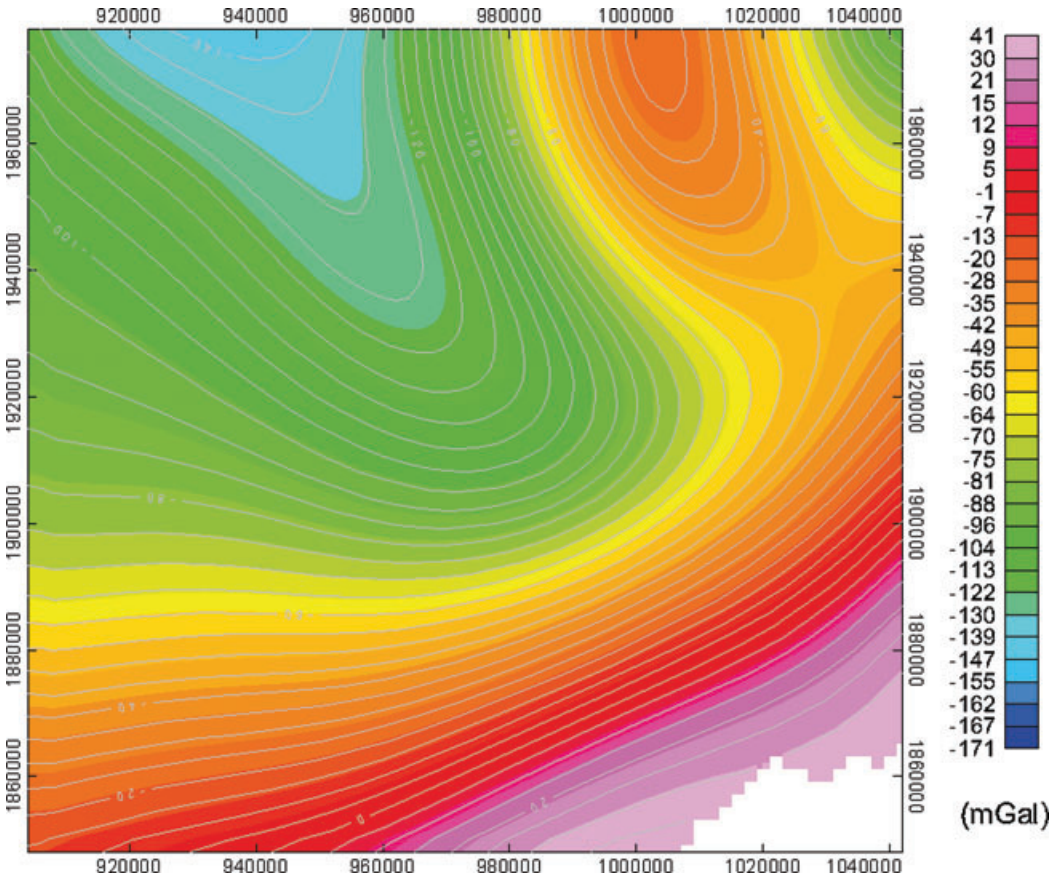

Figure 5. Long wavelength gravity anomaly map of the Southern Alps computed with the 65-km-low-pass filtering. This gravity map represents the gravity signature of the Moho in the studied zone. The Projection is according the Lambert II extended system.

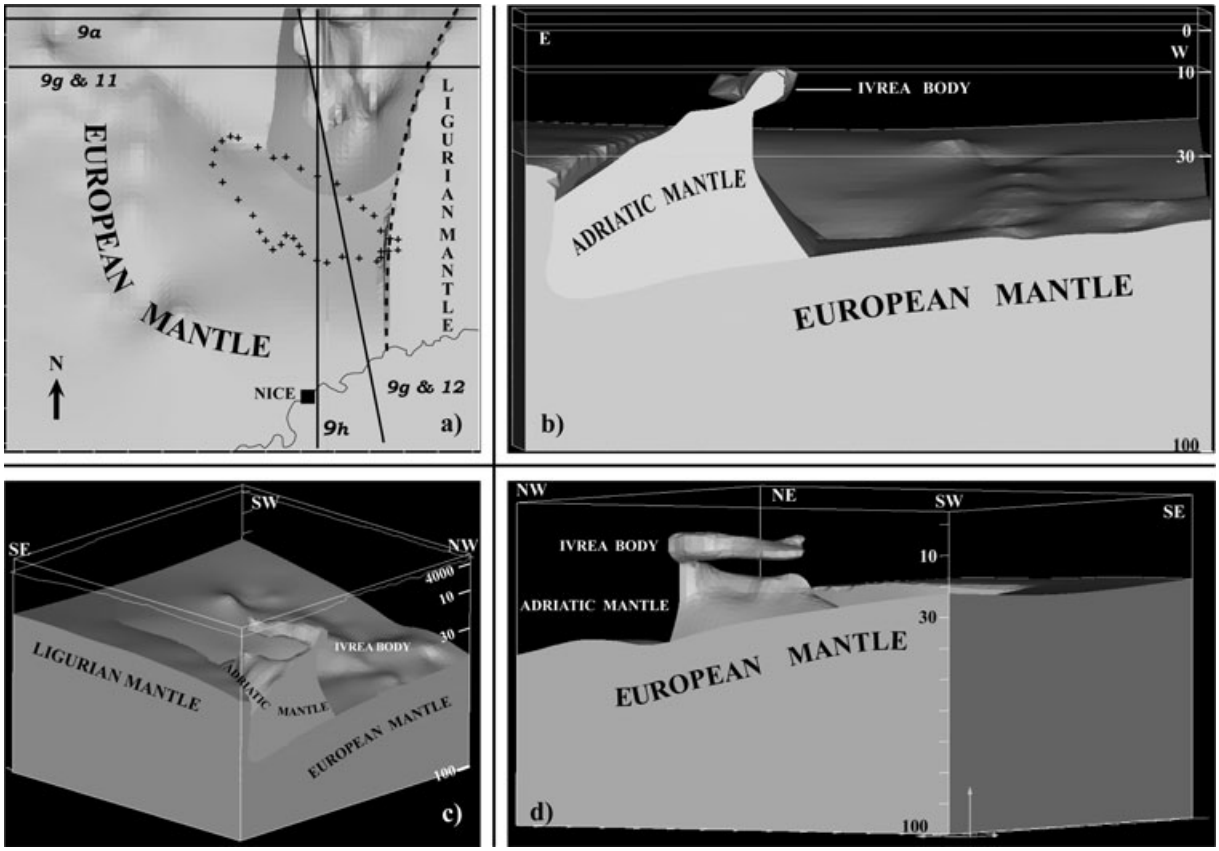

Figure 6. 3-D geometrical model of the superposed Mohos in the Southwestern Alps built from Thouvenot *et al.* (2007) and Waldhauser *et al.* (1998) Moho maps and Paul *et al.* (2001) seismological constraints (*Vp* isovalue equal to 7.0 km s^{-1}). Two layers are presented here: the European mantle, the Adriatic mantle and the Ivrea body. The third layer corresponding to the orogenic crust is not shown in these figures in order to improve their readability. (a) Upper view of the 3-D model. Geological units: Argentera-Mercantour boundaries (black cross). Geographic frame: the French Riviera coast (thin black line); The bold black lines represent the cross-sections traces (E–W; N–S and NNW–SSE) shown in Figs 9, 11 and 12. The black dashed line shows the boundary between the European mantle and the Ligurian mantle after seismic data. (b) View from the north; (c) view from the NE; (d) view from the SW.

decoupling horizon between the upper and the lower part of the European continental crust is not completely excluded in the light of the available seismic constraints. This new configuration based on four modelled layers (Fig. 7) illustrates the subduction of a 20-km-thick piece of lower continental crust, coupled with the European upper mantle, beneath the Ivrea body. Such a configuration was indeed envisaged for different interpretations of seismic reflection profiles in Western and Central Alps (Ménard & Thouvenot 1984; Pfiffner *et al.* 1997; Schmid & Kissling 2000).

In the following sections, we calculate and discuss the gravity signatures of each model (Figs 6 and 7).

4.3 Density model

4.3.1 The three layers model

To calculate the gravity signature of our 3-D models we had to ascribe a density value to each modelled layer: the Ivrea body, the upper mantle and the orogenic crust. For each layer a mean density value was attributed following the rock density calculations of Bousquet *et al.* (1997) and Hyndman & Peacock (2003). For the mantle layer, a density of 3300 kg m^{-3} was used. The choice of a density value for the alpine orogenic crust is more difficult, because variations of lithologies are recognized in the belt. As suggested by different authors (Bousquet *et al.* 1997; Lardeaux *et al.* 2006), the deep architecture of the belt is characterized by the stacking of crustal metamorphosed slices extracted from the subducted European lithosphere. These rocks are metamorphosed probably under blueschist to amphibolite metamorphic facies (Goffé *et al.* 2004) with densities in the range of 2750–2800 kg m^{-3}. In the External Zone, the crust beneath a thin sedimentary layer is composed mainly by Hercynian metamorphic rocks (amphibolite and granulite facies para- and orthogneisses) with a mean density of about 2750 kg m^{-3}. Therefore, we considered a mean density value equal to 2800 kg m^{-3} for the orogenic crust.

The Ivrea body is characterized by a *Vp* velocity interval between 7.0 and 7.4 km s^{-1} (Paul *et al.* 2001; Béthoux *et al.* 2007), which differs from the normal upper mantle velocity of 8 km s^{-1}. As discussed by Paul *et al.* (2001) and Lardeaux *et al.* (2006), a velocity of about 7.0 km s^{-1} is consistent with the mineralogy predicted for this mantle piece located at a shallow depth. Under these depth conditions, the mantle body should be partly serpentinized. In the case of a high degree of serpentinization, the mantle density would be expected to be as low as 3000 kg m^{-3} (Hyndman & Peacock 2003). Following these authors, *P*-wave velocities comprised between 7.4 and 7 km s^{-1} in the upper mantle correspond to 15–30 per cent of serpentinization. For such value, mantle density is considered to be comprised between 3200 and 3000 kg m^{-3}. Mineralogy, seismic velocity and density versus rock composition were also computed by Hacker *et al.* (2003) for different degrees of mantle hydratation. At shallow depths (i.e. around 1 GPa), for around 6 wt% H_2O content in the mantle, serpentine-chlorite mineralogic facies is expected and

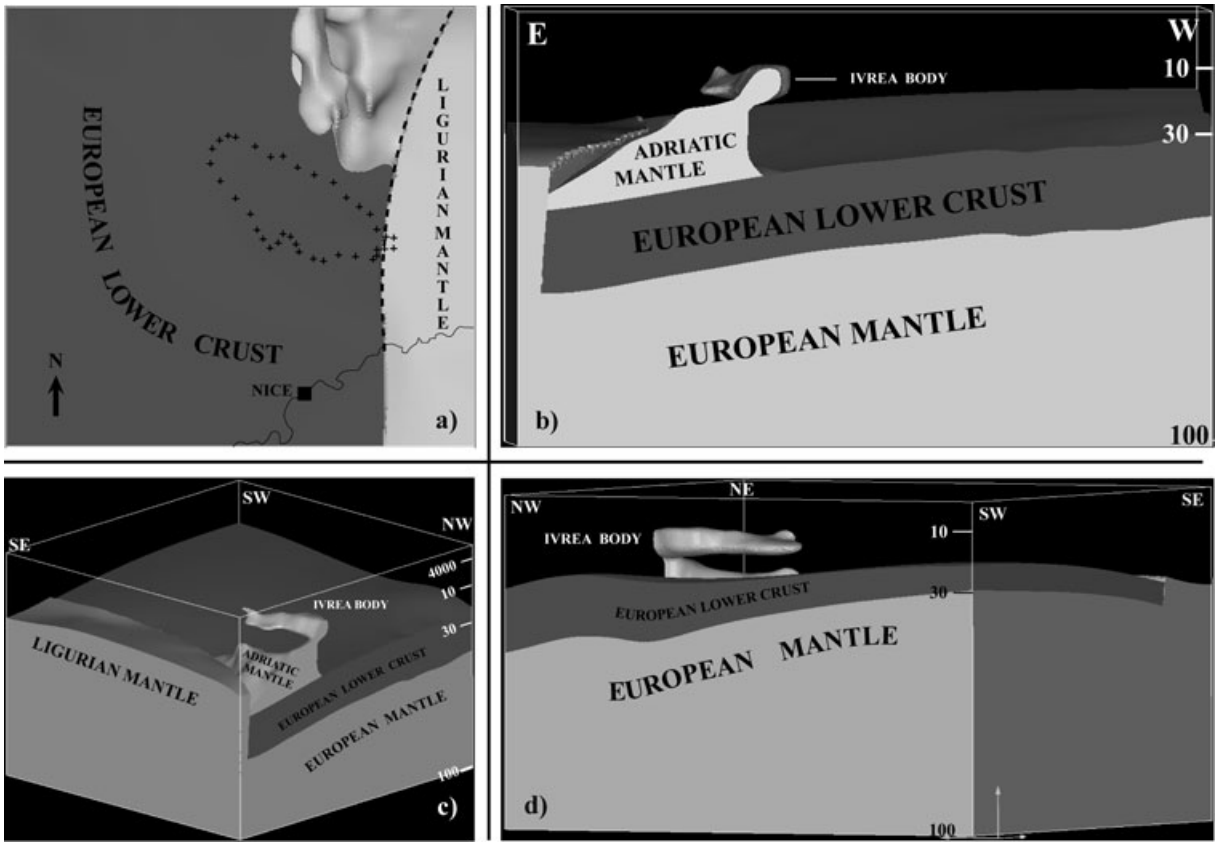

Figure 7. 3-D geometrical model built from Thouvenot *et al.* (2007) and Waldhauser *et al.* (1998) Moho maps and Paul *et al.* (2001) seismological constraints (*Vp* isovalue equal to 7.0 km/s) with a additional layer of subducted continental crust beneath the Ivrea body. Three layers are presented here: the European mantle, the orogenic lower crust, the Adriatic mantle and the Ivrea body. The fourth layer corresponding to the upper orogenic crust is not shown in these figures in order to improve their readability. (a) Upper view of the 3-D model. Geological units: Argentera-Mercantour boundaries (black cross). Geographic frame: the French Riviera coast (thin black line); The black dashed line shows the boundary between the European mantle and the Ligurian mantle after seismic data; (b) View from the north; (c) view from the NE; (d) view from the SW.

mantle densities around 3200 kg m^{-3} are calculated. We have therefore calculated the gravity effect of our model with a density value of the Ivrea body comprised between 3300 and 3000 kg m^{-3}. In our experiences, it appears that a density value of 3230 kg m^{-3} produces the best fit between measured and observed gravity anomalies. This density value was also proposed for the Ivrea body by previous authors in their interpretations of deep seismic reflection profiles in the western Alps (see Marchant & Stampfli (1997) for example).

4.3.2 The four layers model

With respect to the previously presented model we had to ascribe a density value to the new layer of subducted continental crust beneath the Ivrea body. Following the mineralogical models proposed by Bousquet *et al.* (1997), we considered a density range between 2800 and 3000 kg m^{-3} for this piece of underthursted continental crust and the gravity effect was then computed using this density range.

4.4 Gravity signature of our 3-D models

The results of our modelling are presented in Fig. 8. The gravity effects of both three and four layers models were computed and the misfits between the measured and the computed gravity anomalies were calculated (Figs 8a and b).

The first-order gravity shape of the gravity effect of the three layers model (Fig. 8a) is in reasonable agreement with the shape of the observed anomaly. Indeed, the misfit values are comprised between −38 and 67 mGal. Such moderate discrepancies between the observed and calculated gravity anomalies suggest that the proposed Moho geometry is compatible with gravity data.

On the other hand, considering the four layers model (Fig. 7), the misfit of the gravity effect of this model and the available data is significantly degraded whatever the considered density range (Fig. 8b). For a density value from 2800 to 3000 kg m^{-3} the gravity effect generated by the Ivrea body is considerably weakened. This suggests that subduction of continental crust is no more active in the present-day configuration of the Southwestern Alps.

In the following section, we propose thus to invert gravity data to further improved the gravity fit starting from the three layers 3-D model.

5 REFINEMENT OF THE MODEL BY 3-D GRAVITY INVERSION

5.1 Inversion methodology

Having produced a 3-D model of the superposed alpine Mohos, inversion can be used to test the validity of that model with respect to independent data sets. We will discuss how we can statistically

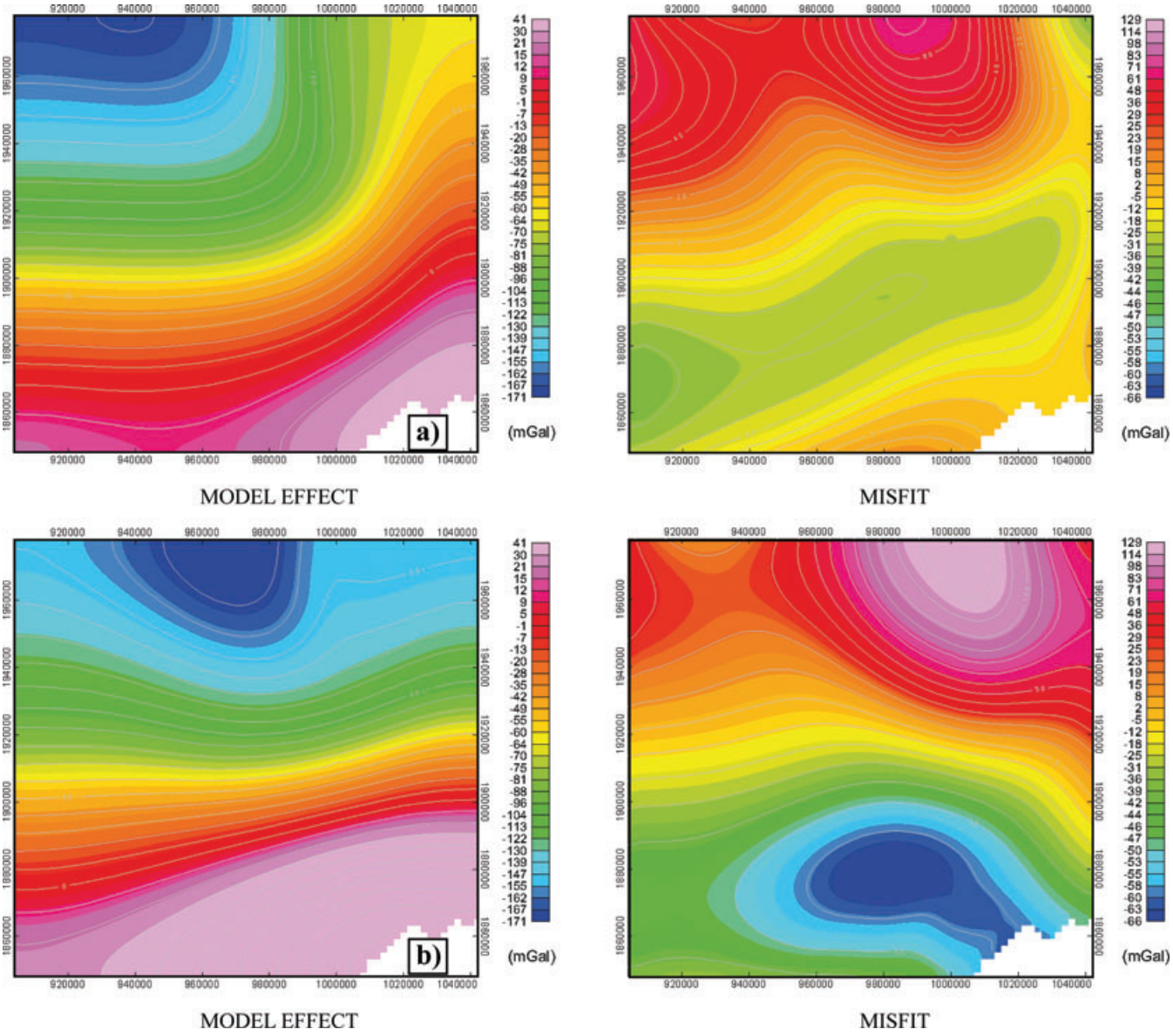

Figure 8. (a) Gravity effect of the 3-D geometrical model presented in Fig. 6 and calculated with density values equal to 3300 kg m^{-3} for the mantle layer, 3230 kg m^{-3} for the Adriatic mantle and 2800 kg m^{-3} for the orogenic crust. The misfit is calculated in comparison with the long wavelenght (the 65-km-low-pass-filtering) gravity anomaly map. (b) Gravity effect of the 3-D geometrical model presented in Fig. 7 and calculated with density values equal to 3300 kg m^{-3} for the mantle layer, 3230 kg m^{-3} for the Adriatic mantle 3000 kg m^{-3} for the orogenic lower crust and 2800 kg m^{-3} for the upper orogenic crust. The misfit is calculated in comparison with the long wavelenght (the 65-km-low-pass-filtering) gravity anomaly map.

estimate the robustness of such 3-D model taking into account variation of gravity data. This estimation can be computed by using complementary data sets, provided that: (i) the data are a function of the 3-D distribution of a gravity source, (ii) the response of a given 3-D source distribution can be calculated and (iii) the source distribution shows some degree of correlation with the litho-regions. Gravity data generally satisfy these criteria, and a 3-D gravity inversion is possible using a probabilistic formulation of the inverse problem (Bosch 1999; Guillen *et al.* 2000, 2008; Bosch & McGaughey 2001). Unfortunately, gravity data do not allow source geometry to be uniquely resolved through inversion, nor is the source geometry likely to be perfectly correlated with the litho-regions (i.e. densities of the different units). Even allowing for these limitations, we can see through the expression for the posterior probability density function (PPD) for a Bayesian inversion procedure how uncertainty in prior geological knowledge is modified by investigating the fit to observed potential field data for various models;

$$P(\mathbf{m} \mid \mathbf{d_o}) = k\rho(\mathbf{m})L(\mathbf{d_o} \mid \mathbf{m}), \quad (1)$$

where k is a normalizing constant, $\rho(\mathbf{m})$ is the prior probability for the property model $\mathbf{m}$ based on geological knowledge, and $L(\mathbf{d_o} \mid \mathbf{m})$ is the likelihood function that reflects the agreement between the observed potential field response and the predicted response of the model. In eq. (1), the prior probability is a measure of the variability in model properties that we allow based on geological/seismological knowledge. Litho-models that have reasonable probability based on prior knowledge are downgraded if the likelihood deduced from the associated potential field response is very low.

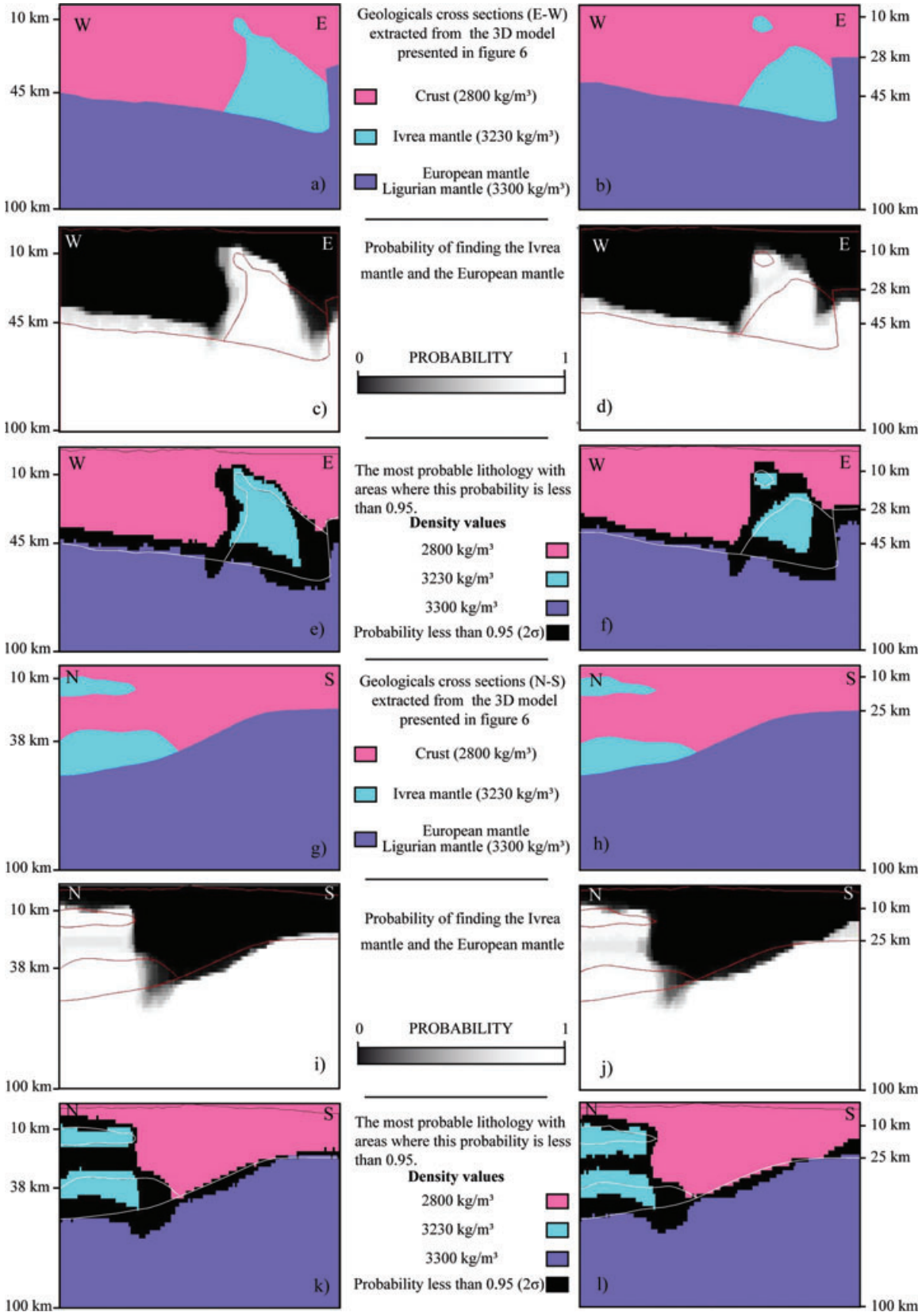

Figure 9. Results of the probalistic inversion process from crustal-scale cross-sections (E–W, N–S and NNW–SSE) extracted and calculated from the 3-D model (Fig. 6). The cross-sections, (a, b, g and h) represent the topology of the starting model shown in Fig. 6. The topology of the starting model is also identified in the other cross sections by red and white lines. Cross-sections (c, d, i and j) calculated from the litho-inversion model show the probability to find the Ivrea body and the European lithospheric mantle whereas (e, f, k and l) cross sections present the distribution of the initial density values within the 95 per cent confidence limits.

5.2 Practical procedure

The geological model is discretized into a 3-D matrix of voxels, to produce an initial rock unit ('lithology') model. Lithology is the primary model parameter. The lithology associated with subsurface voxels information is free to vary, subject to the condition that the topology of the initial model remains unchanged; i.e. no new geological objects are generated or segmented. The inversion explores variations to the initial model, which reproduces the supplied gravity within a desired tolerance level. The adopted strategy is to randomly walk around the space of possible models for a given set of *a priori* information. This approach was proposed by Mosegaard & Tarantola (1995) and developed in 2-D by Bosch & McGaughey (2001).

Many transient models are derived from the initial model using an iterative procedure. At each iteration, occurs one of two possible changes. The physical property (density) for a randomly selected voxel that is separated from the boundary of that unit may be modified. Alternately, the lithology of a voxel that lies on the interface between two or more units may be modified and a new physical property assigned to that voxel according to a random selection from the probability function of the relevant physical property distribution for the new lithology.

The change in the misfit between the observed gravity field data and the responses calculated for the modified model is determined. This change is examined in a probabilistic framework to determine whether the modification to the model is accepted.

During the initial part of the inversion, the data misfit for each field of the current model follows a generally decreasing trend. At some point, the data misfit reaches an asymptotic value, defined or set in function of the measurement errors and start to begin stored. These models are an exploration of the probability space of acceptable models and several millions of such models can be iterated end stored.

Once inversion finished, the set of stored model allows computing, for each voxel, the probability of finding each unit, the most probable lithology and the mean value of the petrophysical properties (see Guillen *et al.* (2008) for a thorough description of the inversion scheme).

5.3 Inversion processing results

The initial alpine Moho model of Fig. 6 was discretized in voxels of 1000 m $\times$1000 m $\times$ 2000 m. The gravity effect of the model was computed using the initial mean density values of 3300 kg m^{-3} for the mantle layer, 2800 kg m^{-3} for the crust and 3230 kg m^{-3} for the Ivrea body, and a standard deviation of 50 kg m^{-3}. This deviation value of the density is used stochastically during the inversion process to modify the density properties of each layer in order to fit with the measured gravity anomaly map along the iterations.

The results of the inversion process are presented in the Figs 9 and 10. The first results (Fig. 9) are provided in terms of probability to find the different lithologies in cross sections (E–W, NNW–SSE and N–S) extracted from the probabilistic inversion 3-D space. The latter allow for small fluctuations in density to exist within each geological unit, as expected in a complex geological system.

The Figs 9(a), (b), (g) and (h) represent two E–W, one NNW–SSE, and one N–S cross-sections located in Fig. 6. The NNW–SSE and N–S cross-sections (Figs 9g and h) enhance the shape of the Ivrea body. The Figs 9(c), (d), (i) and (j) show the probability of finding the Ivrea mantle and the European mantle. In each section, the black

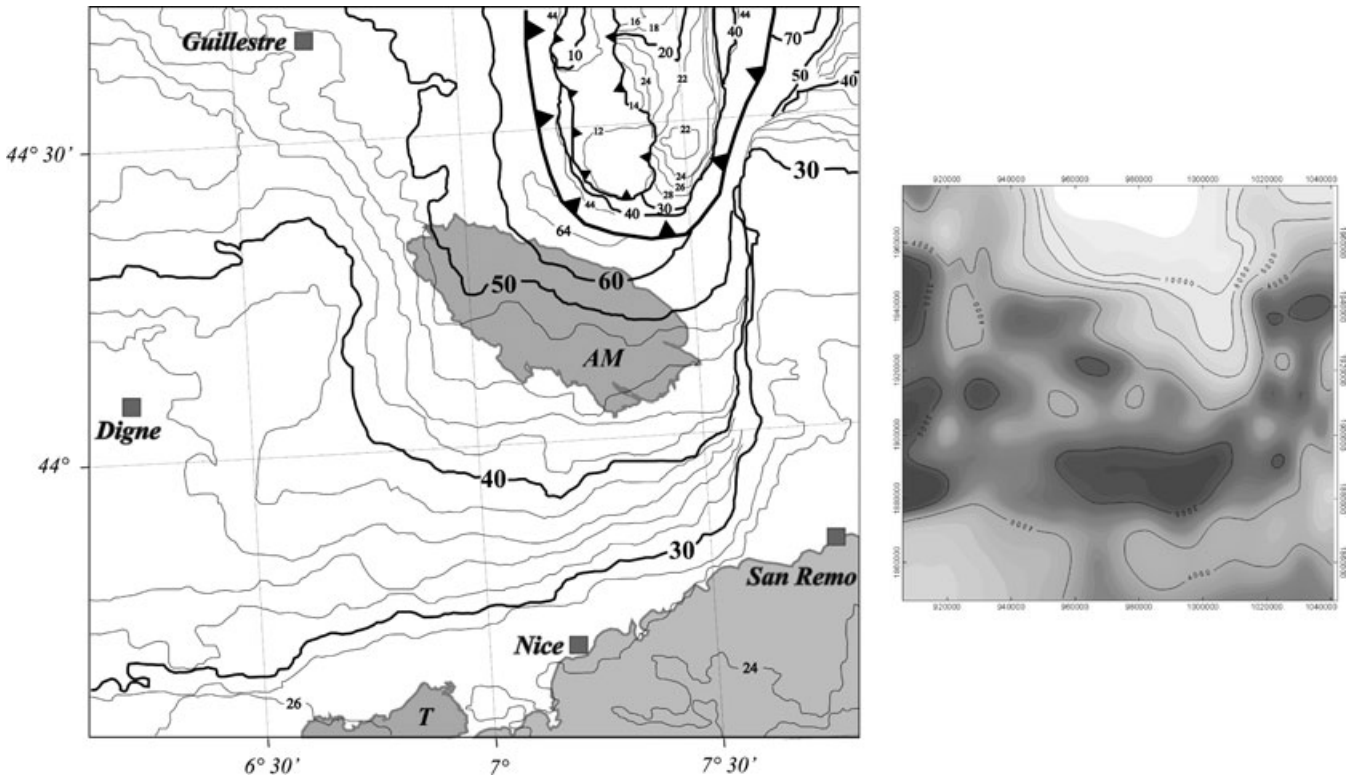

Figure 10. On the left-hand side, probabilistic Moho map of the South Alpine Mohos (2σ). Mapping integrates all the results of the inversion process. Geological units: AM, Argentera-Mercantour massif; T, Tanneron massif. On the right-hand side, map representing the uncertainties of the Moho depth calculated after the spatial distribution of the gravity standard deviation.

area corresponds to a zero probability whilst white area represents a probability of one. Thin red lines represent the lithological boundaries as defined in the starting model of Fig. 6. On Figs 9(e), (f), (k) and (l) the most probable location of the lithological boundaries is shown: black areas correspond to the domains where the probability of occurrence of the lithology is less than 0.95 (2σ). The thin white lines underline the starting geological model.

The results of the inversion process were also used to produce a Moho map (Fig. 10), showing the most probable geometry of Alpine Mohos and the distribution of the uncertainties on the Moho depth. The results of this probalistic inversion are consistent with the crustal 3-D geometry derived in Fig. 6 from seismic and seismological data. The European mantle topography as well as the geometry of the Ivrea body are globally weakly modified during the inversion. In Fig. 9, a continuous Ivrea body can be conclusively distinguished from a discontinuous one. However the best fit model, with 100–95% of probability, supports a discontinuous Ivrea body partly split into two distinct units, the upper unit located at 10 km depth beneath the Dora-Maïra massif, south and west-verging and the lower unit spreading from 20 to 45 km depth. Moreover, the seismological constraints shows that the shape of the Ivrea body remains separated in two pieces in a range *Vp* values from 6.8 to 7.0 km s^{-1} (Paul *et al.* 2001; Béthoux *et al.* 2007). According to Thouvenot *et al.* (2007) the Ivrea body rests upon the European mantle. The latter plunges deeper towards the North beneath the Argentera massif down to 50–60 km depth. Consistent with the conclusions of Waldhauser *et al.* (1998) our probabilistic inversion reveals a sharp boundary between the European and the Ligurian mantle East of Argentera massif (Fig. 10). This variation of the Moho topography reaches a maximum of 20 km east of Argentera massif, and seems to disappear towards the south in the Ligurian basin.

6 DISCUSSION AND CONCLUSIONS

6.1 Consistency of the proposed 3-D model

The 3-D model of Alpine Mohos in the Southwestern Alps proposed as Fig. 6 is the result of the fusion, in a single and coherent 3-D space, of all the available geophysical constraints (seismic and gravimetric databases) obtained in the last 10 yr.

As shown in Fig. 10, the final most probable model derived from gravity inversion validates the 3-D model presented in Fig. 6 and particularly the followings.

(1) The partial splitting of the Ivrea Body into two distinct units.
(2) The thickness of about 50 km for the European continental crust beneath the Argentera-Mercantour massif.
(3) The decoupling of the European upper mantle from the European continental crust at the Alpine root.

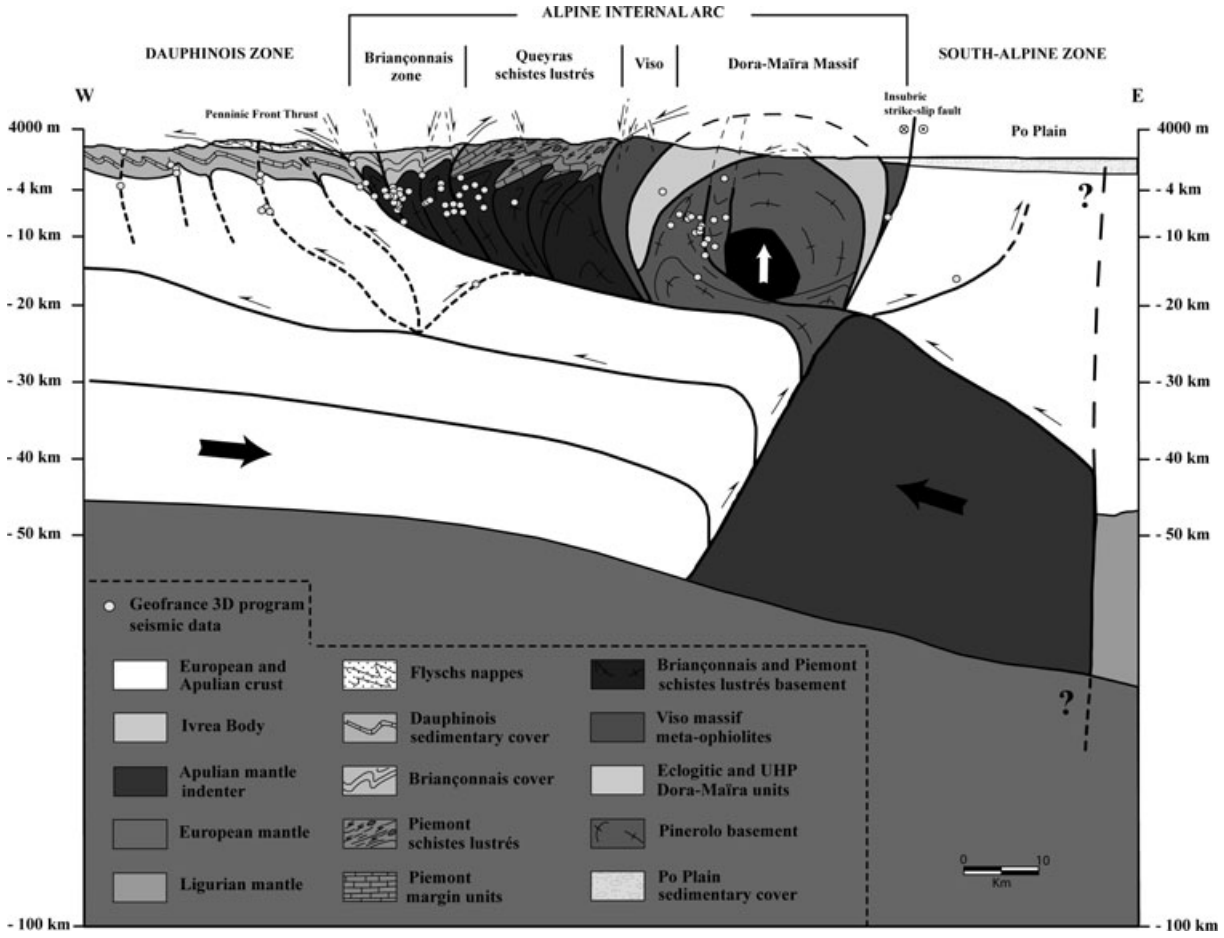

Figure 11. Interpretative crustal-scale cross-sections of the Southwestern Alps (see Fig. 6a for location) drawn from E–W cross-sections extracted from the 3-D probalistic model (Fig. 10). On these cross-sections are show the kinematic indicators and the localization of earthquake hypocentres (dots; Geofrance 3-D (1997) recorded seismicity) with respect to the main geological and tectonic boundaries.

(4) The presence of a boundary between the European and the Ligurian mantle East of Argentera massif previously described by Waldhauser *et al.* (1998).

This new image of the geometry of Alpine Mohos is therefore the 3-D structure, which offers, at the moment, the best consistency between all the geophysical data.

To illustrate the geometry of the Alpine Mohos after refinement by 3-D gravity inversion, we propose a probabilistic Moho map with calculated uncertainties on the Moho depth values according to the gravity standard deviation (Fig. 10).

6.2 Crustal scale structure of the Southwestern Alps and earthquake locations

To precise the 3-D crustal-scale structure of the Southwestern Alps, the main geological units and their tectonic boundaries were extracted from the 1/250 000 maps of Gap and Nice (Rouire *et al.* 1980) and imported in our 3-D model (Fig. 10). Two, subperpendicular (E–W and NNW–SSE), crustal scale cross-sections (see localization on Fig. 6) were constructed and are presented in Figs 11 and 12.

A subdivision of the Ivrea Body into two distinct pieces is highly probable and constitutes a prominent result of our 3-D model. The two rigid pieces of Apulian mantle play a significant role in the development and localisation of crustal strain in the area of interest. In our cross-sections, the lowermost piece of the Apulian mantle acts as a mantle identer which tranfers the compression towards the external Alpine Zone. Therefore, it corresponds to the 'mantle backstop' (Fig. 11) of the Oligocene Alpine collision (see Vialon *et al.* 1989; Ford *et al.* 2006 for discussion). On the other hand, the uppermost piece of the Apulian mantle (Ivrea Body) represents a second mechanical heterogeneity still pushing the crust southward, leading to the localization of thrusts and folds systems during the Mio-Pliocene to current NNW–SSE crustal shortening described in the Southwestern Alps (Giannerini *et al.* 1977; Campredon & Giannerini 1982; Ritz 1991; Bigot-Cormier *et al.* 2004).

In the NNW–SSE crustal scale cross-sections (Fig. 12), we also localized, the predictive Moho depth obtained by Bertrand & Deschamps (2000) (Fig. 2a) after receiver function modelling at the SAOF station. Their prediction appears under-estimated compared to the Moho map presented on Fig. 12. As the Bertrand & Deschamps (2000) conclusions relies on synthetics seismograms computed for a flat layered crustal model, which is clearly not the case in the area of interest we consider that their Moho depth estimate is insufficiently constrained. Nevertheless, it is possible to interpret the significant change in the P-wave velocity structure of the lithosphere observed at 20 km by Bertrand & Deschamps (2000) as an intracrustal decoupling horizon instead of the Moho.

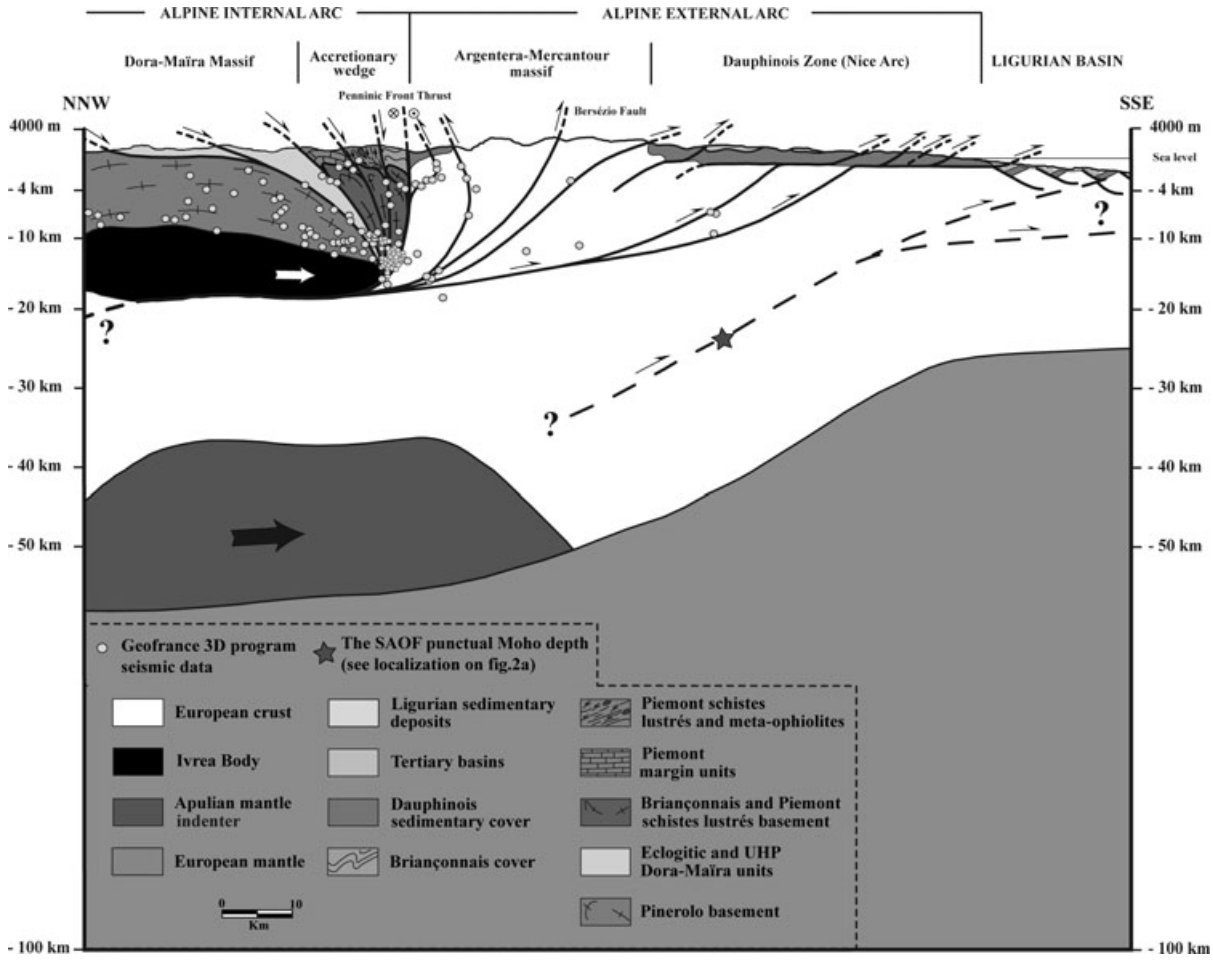

Figure 12. Interpretative crustal-scale cross-sections of the Southwestern Alps (see Fig. 6a for location) drawn from NNW-SSE cross-sections extracted from the 3-D probalistic model (Fig. 10). On these cross-sections are shown the kinematic indicators and the localization of earthquake hypocentres (dots; Geofrance 3-D (1997) recorded sismicity) with respect to the main geological and tectonic boundaries.

The seismological database (see Béthoux *et al.* (2007)) established in the framework of the GéoFrance 3-D research program (1998–2003) were also integrated in the 3-D model and earthquakes hypocentres were located with respect to the crustal scale structures. The earthquakes hypocentres were then projected in these two cross sections taking into account a data projected radius equal to 10 km.

In the E–W cross-section (Fig. 11), in the Dauphinois zone, earthquake hypocentres are localized on the thrust zones or inverse faults, which accommodate the crustal shortening of the European foreland. Earthquake hypocentres are localized mainly on the Penninic Frontal Thrust (PFT) and/or on its reactivated segments during present-day extension tectonics (Sue & Tricart 1999; Sue & Tricart 2003; Tricart *et al.* 2004, 2006). Another seismic zone corresponds clearly to the Briançonnais backthrust structure Briançonnais backfolds and backthrusts, (Tricart 1984; Sanchez *et al*. in press) reactivated today by strike-slip tectonics. In the Piedmont zone, the seismicity is clearly controlled by the position of the upper rigid mantle piece, the earthquake hypocentres being mainly observed at the front of the Apulian mantle indenter. In the Southalpine zone, a restricted number of hypocentres are associated to the Insubric strike-slip system (see also Béthoux *et al.* 2007).

In the NNW–SSE cross-section (Fig. 12), the distribution of earthquake hypocentres is, in a spectacular way, controlled by the position of the uppermost rigid mantle unit. Indeed, a majority of hypocentres are localized on the subvertical tectonic structures developed at the front mantle identer, while a restricted number of hypocentres underline the main Southverging basal thrust, beneath the Argentera-Mercantour massif, considered by several authors (Béthoux *et al.* 1988; Chaumillon *et al.* 1994; Bigot-Cormier *et al.* 2004) as the tectonic structure accommodating the inversion of the Ligurian margin.

We can therefore conclude that in the Southwestern Alps the seismicity is strongly controlled by tectonic crustal scale structures and particularly the position of the Apulian upper mantle. The seismicity is located in the brittle upper part of the orogenic crust bounded by the main basal shear plane (Alpine sole thrust) still active today (Figs 11 and 12).

ACKNOWLEDGMENTS

We gratefully acknowledge two anonymous reviewers and Saskia Goes for their helpful comments. We wish to thank P. Ledru, P. Calcagno, N. Béthoux, E, Tric, Y. Rolland, G. Sanchez and G. Giannerini for constructive discussions. Finally, we acknowledge A. Paul for exchange of ideas and for the tomographic database.

REFERENCES

Bertrand, E. & Deschamps, A., 2000. Lithospheric structure of the southern French Alps inferred from broadband analysis, *Phys. Earth planet. Inter.,* **122,** 79–102.

Béthoux, N., Cattaneo, M., Delpech, P.-Y., Eva, C. & Rehault, J.-P., 1988. Mécanismes au foyer de séismes en Mer Ligure et dans le sud des Alpes occidentals: résultats et interpretations, *C. R. Acad. Sci. Paris,* **307**(11), 71–77.

Béthoux, N., Sue, C., Paul, A., Virieux, J., Fréchet, J., Thouvenot, F. & Cattaneo, M., 2007. Local tomography and focal mechanisms in the Southwestern Alps: comparison of methods and tectonic implications, *Tectonophysics,* **432,** 1–19.

Bigi, G., Castellarin, A., Coli, M., Dal Piaz, G.V., Sartori, R., Scandone, P. & Vai, G.-B., 1990. Structural model of Italy, in *Progetto Finalizzato Geodinamica,* C.N.R., Firenze.

Bigot-Cormier, F., Sage, F., Sosson, M., Dèverchére, J., Ferrandini, M., Guennoc, P., Popoff, M. & Stéphan, J.-F., 2004. Pliocene deformation of the north-Ligurian margin (France): consequences of a south-Alpine crustal thrust, *Bull. Soc. Géol. Fr.,* **175,** 197–211.

Bosch, M., 1999. Lithologic tomography: from plural geophysical data to lithology estimation, *J. geophys. Res.,* **104,** 749–766.

Bosch, M. & McGaughey, J., 2001. Joint inversion of gravity and magnetic data under lithologic constraints, *Leading Edge,* **20,** 877–881.

Bousquet, R., Goffé, B., Henry, P. & Chopin, C., 1997. Kinematic, thermal and petrological model of the Central Alps: Lepontine metamorphism in the upper crust and eclogitisation of the lower crust, *Tectonophysics,* **273,** 105–127.

Calcagno, P., Chilès, J.P., Courrioux, G. & Guillen, A., 2008. Geological modelling from field data and geological knowledge. Part I: modelling method coupling 3-D potential-field interpolation and geological rules, *Phys. Earth planet. Inter.,* **171,** 147–157.

Campredon, R. & Giannerini, G., 1982. Le synclinal de Saint Antonin (arc de Castellane, chaînes subalpines méridionales). Un exemple de bassin soumis à une déformation compressive permanente depuis l'Eocène supérieur, *Géologie Alpine,* **58,** 15–20.

Chaumillon, E., Deverchére, J., Réhault, J.-P. & Gueguen, E., 1994. Réactivation tectonique et flexure de la marge continentale ligure (Méditerranée occidentale), *C. R. Acad. Sci. Paris,* **319,** 675–682.

Closs, H. & Labrouste, Y., 1963. Recherces séismologiques dans les Alpes occidentales au moyen de grandes explosions en 1956, 1958 et 1960, *Mem. Coll. Ann. Géophys. Int.,* **12,** 241pp., CNRS, Paris.

Coward, M.P. & Dietrich, D., 1989. Alpine tectonics; an overview, *Geological Soc. Special Pub.,* **45,** 1–29.

Ford, M., Duchêne, S., Gasquet, D. & Vanderhaeghe, O., 2006. Two-phase orogenic convergence in the external and internal SW alps, *J. Geol. Soc., Lond.,* **163,** 815–826.

Giannerini, G., Gigot, P. & Campredon, R., 1977. Le tertiaire de la Roque-Esclapon (front sud de l'arc de Castellane): la superposition de deux deformations synsédimentaires Oligocène et Miocène et des basins sédimentaires associés, *Bull. BRGM, Fr.* (2), Section 1, no. 3, 179–188.

Goffé, B., Schwartz, S., Lardeaux, J.M. & Bousquet, R., 2004. Metamorphic structures of the western and Ligurian Alps, *Mitt. Osterr. Mineral. Ges.,* **149,** 125–144.

Grandjean, G., Ménnechet, C., Debéglia, N. & Bonijoly, D., 1998. Insuring the quality of gravity data, *EOS, Trans.–Am. geophys. Un.,* **79,** 217–221.

Grellet, B., Combes, P., Granier, T. & Philip, H., 1993. *Sismotectonique de la France métropolitaine dans son cadre géologique et géophysique,* Vol. 164, Mém. Hors-Sér. Soc. géol.

Groupe de recherche GéoFrance 3-D, 1997. GéoFrance 3-D: l'imagerie géologique et géophysique du sous-sol de la France, *Mém. Soc. géol. Fr,* **172,** 53–71.

Guillen, A., Calcagno, P., Courrioux, G., Joly, A. & Ledru, P., 2008. Geological modelling from field data and geological knowledge. Part II: modelling validation using gravity and magnetic data inversion, *Phys. Earth planet. Inter.,* **171,** 158–169.

Guillen, A., Delos, V. & Ledru, P., 2000. A new method to determine lithology and geometry in depth: 3-D litho-inversion of potential fields. in *25th General Assembly,* pp. abstract, ed. Society, E.G., Katlenburg-Lindau, Federal Republic of Germany (DEU).

Hacker, B.R., Abers, G.A. & Peacock, S.M., 2003. Subduction factory 1. Theoretical mineralogy, densities, seismic wave speeds, and H_2O contents, *J. geophys. Res.,* **108,** doi:10.1029/2001JB001127.

Hyndman, R.D. & Peacock, S.M., 2003. Serpentinization of the forearc mantle, *Earth planet. Sci. Lett.,* **212,** 417–432.

Lardeaux, J.M., Schwartz, S., Tricart, P., Paul, A., Guillot, S., Béthoux, N. & Masson, F., 2006. A crustal-scale cross-section of the southwestern Alps combining geophysical and geological imagery, *Terra Nova,* **18**(6), 412–422.

Marchant, R.H. & Stampfli, S.M., 1997. Crustal and lithospheric structure of the Western Alps. in *Deep Structure of the Swiss Alps: Results of NFP20,* pp. 326–337, ed. Pfiffner, O.A. *et al*., Birkhauser, Basel.

Martelet, G., Calcagno, P., Gumiaux, C., Truffert, C., Bitri, A., Gapais, D. & Brun, J.P., 2004. Integrated 3-D geophysical and geological modelling of the Hercynian Suture Zone in the Champtoceaux area (south Brittany, France), *Tectonophysics,* **382,** 117–128.

Martelet, G., Debéglia, N. & Truffert, C., 2002. Homogénéisation et validation des corrections de terrain gravimétriques jusqu'à la distance de 167 km sur l'ensemble de la France, *Comptes Rendus Géoscience,* **334,** 449–454.

Masson, F., Verdun, J., Bayer, R. & Debeglia, N., 1999. Une nouvelle carte gravimétrique des Alpes occidentales et ses conséquences structurales et tectoniques, *C. R. Acad. Sci. Paris,* **329,** 865–871.

Ménard, G., 1979. Relations entre structures profondes et structures superficielles dans le Sud-Est de la France. Essai d'utilisation de données géophysiques, *Thèse de 3e Cycle*, Grenoble.

Ménard, G. & Thouvenot, P., 1984. Ecaillage de la lithosphère européenne sous les Alpes Occidentales; arguments gravimétriques et sismiques liés à l'anomalie d'Ivrea, *Bulletin de la Société Géologique de France,* **26,** 875–884.

Mosegaard, K. & Tarantola, A., 1995. Monte Carlo sampling of solutions to inverse problems, *J. geophys. Res.,* **100**(B7), 12 431–12 477.

Paul, A., Cattaneo, M., Thouvenot, F., Spallarossa, D., Béthoux, N. & Fréchet, J., 2001. A three-dimensional crustal velocity model of the southwestern Alps from local earthquake tomography, *J. geophys. Res,* **106,** 19 367–19 389.

Pfiffner, O.A., Lehner, P., Heitzmann, P., Mueller, S. & Steck, A., 1997. *Deep Structure of the Swiss Alps: Results of NRP 20,* pp. 380, Birkhäuser, Basle.

Ritz, J.F., 1991. Evolution du champ de contraintes dans les Alpes du Sud depuis la fin de l'Oligocène: implications sismotectoniques, 3e Cycle, *PhD thesis*. University of Monpellier II, France.

Rouire, J., Autran, A., Prost, A., Rossi, P. & Rousset, C., 1980. Notice explicative de la feuille Nice au 1/250 000 eBureau de Recherches Géologiques et Minières, Orléans.

Roure, R., Polino, R. & Nicolich, R., 1990. Early Neogene deformation beneath the Po Plain: constraints on the post-collisional Alpine evolution, *Mem. Soc. Geol. Fr.,* **156,** 309–321.

Roure, F., Choukroune, P. & Polino, R., 1996. Deep seismic reflection data and new insights on the bulk geometry of mountain ranges, *C. R. Acad. Sci. Paris,* **322**(2a), 345–359.

Sanchez, G., Rolland, Y., Schreiber, D., Giannerini, G., Corsini, M. & Lardeaux, J.-M., The active fault system in of SW Alps, *J. Geodyn.,* doi:10.1013/j.jog.2009.11.009.

Sapin, M. & Hirn, A., 1974. Results of explosion seismology in the southern Rhone valley, *Ann. Géophys.,* **30,** 181–202.

Schmid, S.M. & Kissling, E., 2000. The arc of the western Alps in the light of geophysical data on deep crustal structure, *Tectonics,* **19,** 62–85.

Spector, A. & Grant, F.S., 1970. Statistical models for interpreting aeromagnetic data, *Geophysics,* **35**(2), 293–302.

Sue, C. & Tricart, P., 1999. Late Alpine brittle extension above the Frontal Pennine Thrust near Briançon, Western Alps, *Eclogae Geol Helvet,* **92,** 171–181.

Sue, C. & Tricart, P., 2003. Neogene to ongoing normal faulting in the inner western Alps: a major evolution of the late alpine tectonics, *Tectonics,* **5,** 1–25.

Thouvenot, F. & Perrier, G., 1980. Seismic evidence of a crustal overthrust in the western Alps, *Pageoph,* **119,** 163–184.

Thouvenot, F., Paul, A., Fréchet, J., Béthoux, N., Jenatton, L. & Guiguet, R., 2007. Are there really superposed Mohos in the southwestern Alps? New seismic data from fan profiling reflections, *Geophys. J. Int.,* **170,** 1180–1194.

Tricart, P., 1984. From passive margin to continental collision: a tectonic scenario for the western Alps, *Am. J. Sci.,* **284,** 97–120.

Tricart, P., Schwartz, S., Sue, C. & Lardeaux, J. M., 2004. Evidence of synextension tilting and doming during final exhumation from multistage faults (Queyras, Schistes lustrés, western Alps), *J. Struct. Geol,* **26,** 1633–1645.

Tricart, P., Lardeaux, J.M., Schwartz, S. & Sue, C., 2006. The late extension in the inner western Alps: a synthesis along the south-Pelvoux transect, *Bulletin de la Societe Geologique de France,* **177,** 299–310.

Vernant, P., Masson, F., Bayer, R. & Paul, A., 2002. Sequential inversion of local earthquake traveltimes and gravity anomaly—the example of the western Alps, *Geophys. J. Int.,* **150,** 79–90.

Vialon, P., Rochette, P. & Ménard, G., 1989. Indentation and rotation in the western Alpine arc, *Spec. Publ. Geol. Soc. Lond.,* **45,** 329–338.

Waldhauser, F., Kissling, E., Ansorge, J. & Mueller, S., 1998. Three-dimensional interface modelling with two-dimensional seismic data: the Alpine crust-mantle boundary, *Geophys. J. Int.,* **135,** 264–278.